Hindawi
International Journal of Antennas and Propagation
Volume 2021, Article ID 5524732, 16 pages
https://doi.org/10.1155/2021/5524732

Research Article

Research on Permanent Magnet-Type Super-Low-Frequency Mechanical Antenna Communication

Xiaoyu Wang,[1] **Wenhou Zhang**,[1] **Xin Zhou**,[1] **Zhenxin Cao**,[2] **and Xin Quan**[2]

[1]*College of Mechanical Engineering, Dalian Jiaotong University, Dalian 116045, China*
[2]*College of Information Science and Engineering, Southeast University, Nanjing 211189, China*

Correspondence should be addressed to Xiaoyu Wang; 99925010@qq.com

Received 24 February 2021; Accepted 3 May 2021; Published 13 May 2021

Academic Editor: Mauro Parise

In the super-low-frequency (30 ~ 300 Hz) band communication, the traditional antenna covers a large area and has low radiation efficiency. The excitation of electromagnetic waves by the mechanical motion of permanent magnets enables miniaturized technology for super-low-frequency communication. For this miniaturization technique, this paper proposes a super-low-frequency communication architecture framework. Theoretical analysis and experimental verification of each unit module in the structural framework are carried out to achieve high-quality communication. For the radiation unit, permanent magnet parameters and communication distances are introduced to establish a rotating permanent magnet radiation power analysis model and to study the radiation characteristics of rotating permanent magnets. For the receiver unit, a sensitivity normalization characterization method based on the ratio of the coil thermal noise voltage to the induced voltage is proposed. Based on the sensitivity analysis model, a square coil was developed that meets the communication requirements of a mechanical antenna and an experimental platform was built. Experiments are conducted on the factors affecting radiated power and coil sensitivity, and 2FSK signal modulation communication experiments are conducted to verify the feasibility of the communication structure framework. The volume of the mechanical antenna permanent magnets in the experiment is all below 10 cm^3, and the operating frequency is continuously adjustable from 0 to 250 Hz. The experimental results show that the near-field radiated power of a rotating permanent magnet is proportional to square of the volume of the rotating permanent magnet; the sensitivity of the coil is proportional to the number of turns and the area of the coil. By controlling the speed in real time, you can control the frequency of the signal and modulate it.

1. Introduction

Super-low-frequency (SLF) electromagnetic waves (30 Hz~300 Hz) have excellent seawater penetration and diffraction capabilities, low path loss in water and soil, and strong anti-interference ability. Therefore, super-low-frequency electromagnetic waves are used in the submarine command, mine emergency, earthquake prediction, and penetration. Terrestrial communications and other fields have colossal application potential [1]. In recent years, it has received widespread attention and is also an effective means to realize submarine communication [2].

In practical applications, the existing transmitting antennas are all electrically small antennas (ESAs), which rely on the oscillating current in the conductor to excite electromagnetic waves. ESA is an antenna whose size is small compared to the wavelength of electromagnetic waves in the frequency band in which it works, and generally its size satisfies $(l/\lambda) \leq (1/2\pi)$ [3, 4]. Nowadays, there are mainly three kinds of common electric small antennas, which are electric oscillator-type antenna, magnetic oscillator-type antenna and combination-type antenna. They are achieved through the integrated use of composite structural materials, multipoint feeds, coaxial chokes, and other technologies [5, 6]. The bandwidth and gain of the antenna can be increased by these techniques.

Due to the length of the electric small antenna is much smaller than the working wavelength, its equivalent resistance is often very small, and its reactance part dominates in its impedance, making the change of frequency has a great

impact on the antenna input impedance. Chu et al. [7, 8] gave a theoretical limit of ESA based on the radiation quality factor Q_{rad}: the smaller the antenna size, the larger the Q_{rad}, and the lower the antenna radiation power and radiation efficiency under certain radiation power conditions. Due to the abovementioned theoretical limitations, the radiation performance of ESA is directly limited by the antenna size, so that existing low-frequency electromagnetic transmission systems have problems such as bulky antennas, complex equipment, low radiation efficiency, massive transmission power, and energy consumption.

To address these issues, in February 2016, the Defense Advanced Research Projects Agency (DARPA) first proposed the concept and project idea of a "mechanical antenna" (MA) to replace the traditional ESA that relies on oscillating current excitation [9, 10]. The MA excites and emits super-low-frequency electromagnetic waves by driving an electric dipole or magnetic dipole. MA has opened up a new possible way for the radiation of super-low-frequency electromagnetic waves [11, 12].

Motivated by related projects, several universities and research institutes at home and abroad have conducted preliminary research and exploration of mechanical antennas. Under the same conditions, electrets have higher radiation efficiency than permanent magnets. However, there are technical difficulties in generating a stable, continuous, and high-density static charge on the electret. Therefore, many researchers have chosen rotating permanent magnets as the mechanical antenna transmitting module. The study [13] presented a patent describing a novel antenna for generating low-frequency electromagnetic waves from rotating permanent magnets. In 2017, Madanayake proposed an underwater positioning system consisting of at least three mechanical antennas as reference points and a multidimensional vector magnetometer on the uncrewed underwater vehicle (UUV) as a receiver. Madanayake et al. derived the formula for the magnetic field of a mechanically rotating dipole by assuming that the magnetic field generated by a time-varying dipole has the same spatial distribution as that generated by a static dipole [14] but did not study it experimentally. In 2017, Huang concluded that the spin magnet system is not subject to the Chu Harrington limit in ULF communication and obtained the electromagnetic field formula for the far field [15]. However, the spin permanent magnet, as an ULF mechanical antenna radiation unit with an extremely long wavelength, is more relevant for the near field. In 2018, Gong et al. derived the formula for the electromagnetic field of a rotating permanent magnet in space [16]. Chen et al. discussed the radiation of electric dipoles for this particular motion of uniform rotation [17], which were well deduced from their theory, but not further studied in conjunction with practical situations or simulations.

The "mechanical antenna" project consists of two technical fields (TA1 and TA2), which are divided into three phases (Phase 1~Phase 3) to reduce the difficulty of realization. The time-varying magnetic field strength during steady-state operation of the three phases of TA1 is 1~100 fT@1 km, while the magnetic field strength signal of the fT level is very weak. Highly sensitive magnetic sensors are required for reception. In the field of magnetic sensor technology today, there are mainly magnetic induction coils, optical pump magnetometers, proton (nucleon) spin-in magnetometers, and superconducting quantum interference magnetometers with resolutions up to the pT level [18, 19]. Magnetic induction coils are used in mechanical antenna receiving units because of their simple structure, low power consumption, stable performance, and high resolution [20]. Domestic and international scholars have done a lot of beneficial research for the establishment of an accurate mathematical model for the transmission characteristic analysis of magnetic induction coils in the super-low-frequency domain. They mainly focus on the accurate calculation of the equivalent electrical characteristics parameters (equivalent resistance R, equivalent inductance L, and equivalent capacitance C), the signal-to-noise ratio of the coil, and its feasibility in the low-frequency field.

In order to accurately calculate the equivalent inductance, resistance, and capacitance of the coil, many scholars have done a lot of beneficial research. Zhang established the transfer function of the coil based on the theoretical model of the equivalent circuit of the coil, improved the computational model of the equivalent capacitance, predicted the characteristics of the coil such as resonant frequency, transfer function, and sensitivity, and verified the accuracy of the model through experiments [21], but the study of the parameters of the equivalent electrical characteristics mainly focused on the high-frequency spectral band and did not discuss in detail in the super-low-frequency domain. For the study of methods to improve the signal-to-noise ratio of coils, Slawomir Tumanski analyzed the principle and characteristics of different winding methods of coils and proposed a coil design and parameter optimization method that takes into account both signal-to-noise ratio and sensitivity [22]. To address the feasibility of coils in the low-frequency domain, Burch et al. designed a receiver consisting of a three-axis orthogonal coil and a 24 bit acoustic frequency data recording card, and analyzed the positioning effect of the receiver both theoretically and experimentally, demonstrating that it is feasible and practical at frequencies below 500 Hz and at distances greater than 100 m [23].

In this work, based on a new signal generation and radio transmission mechanism, a mechanical antenna structure is proposed, which mainly includes a signal transmitting module and a signal receiving module. Based on the signal transmitting module, an analytical model of the rotating permanent magnet radiation power is established. Based on the signal receiving module, a coil is selected as a magnetic sensor to receive the signal based on the radiation intensity of the radiated field source. For coil magnetic sensors, a sensitivity normalized characterization method based on the ratio of the coil-induced electric potential force to the thermal noise voltage is proposed. In this paper, a prototype SLF communication principle is developed based on the coil sensitivity model and radiated power model. The correctness of the analytical model and the feasibility of 2FSK communication are verified by conducting experiments with the developed prototype.

2. Mechanical Antenna Communication Model System

2.1. Mechanical Antenna Structure. Super-low-frequency mechanical antennas generate signals through the mechanical vibration of permanent magnets or electrets to transmit super-low-frequency radio waves. The electrets or permanent magnets are the core radiating components of the mechanical antenna. Electret and permanent magnet can be equivalent to electric dipole and magnetic dipole, respectively. According to Coulomb's law, an electret is equivalent to a collection of charges, which can be equated to an energized coil; a permanent magnet is equivalent to a collection of magnetic dipoles, which can be equated to two charged planes. The mechanical antenna field source model is selected by comparing the ability of the two equivalent models to produce magnetic field strengths. The model parameters of permanent magnet and energized coil are shown in Table 1.

The model of permanent magnet and the energized coil are shown in Figure 1. The magnetization intensity of permanent magnet is $M = 1.1 \times 10^6$ A/m, and the calculation formula of magnetic field intensity H is

$$H = N \times \frac{I}{L}, \tag{1}$$

where N is the number of turns of the excitation coil; I is the excitation current; and L is the effective magnetic circuit length of the excitation coil.

According to formula (1), an excitation coil with a wire diameter of 12AWG and a number of turns of 330 applying an excitation current of 100 A can radiate a magnetic field strength of $H = 1.1 \times 10^6$ A/m. However, the 12AWG coil can withstand the maximum current of 14.9 A. Therefore, eight energized coils of the same size would be required to apply a current of 12.5 A to radiate a magnetic field strength of $H = 1.1 \times 10^6$ A/m. Therefore, in this paper, permanent magnets are chosen as the radiating unit of the super-low-frequency mechanical antenna.

To better control the drive motor and receive communication signals, a mechanical antenna structure is proposed as shown in Figure 2, which mainly includes a signal transmitting module and a signal receiving module. The signal transmitting module is mainly composed of radiation field source (permanent magnet), drive motor, power converter, controller, and signal generator. The signal generator sends the signals required for communication to the inverter and power converter. The inverter outputs signals to control the speed of the drive motor. The drive motor drives the permanent magnet to generate a time-varying magnetic field, which radiates electromagnetic waves. The signal receiving module is mainly composed of a magnetic sensor and a preamplifier. The magnetic sensor receives the time-varying magnetic field signal and processes the signal through the preamplifier to obtain the communication signal and complete the mechanical antenna communication.

2.2. Information Loading Module and Its Speed Control Method. Unlike high-frequency carrier systems, super-low-frequency carrier communication systems typically have a narrower bandwidth but are less susceptible to outside interference. As a super-low-frequency communication navigation transmitter system, the modulation methods used are mainly divided into amplitude modulation, frequency modulation, and phase modulation. However, due to the extremely long operating wavelength of SLF communication systems, which usually operate in non-far-field regions, amplitude modulation information is complex and not easily demodulated. Phase modulation requires precise control of the motor's rotational attitude at different times. This is difficult to achieve for super-high-speed motors running at 10,000 rpm or more. Therefore, frequency modulation is used for SLF mechanical antenna communication modulation.

Frequency modulation currently uses constant envelope modulation methods such as FSK and MSK. Mechanical antennas load the information by changing the state of the rotational motion of the field source. Therefore, the frequency parameters need to be mapped to the rotational state of the field source to generate the input parameters of the rotating servo system.

In order to realize the information loading of FSK, this paper proposes an information loading method based on the field source rotation speed n control, which maps the frequency modulation to the control of the average rotation speed $\overline{n}$. Taking 2FSK as an example, Figure 3 is based on $\overline{n}$ control and shows a schematic diagram of generating corresponding control signals based on code data.

2.3. Energy Conversion of Mechanical Antenna. The rotation servo system of the mechanical antenna converts the input electric power P_{in} into the rotating torque of the field source, the electromagnetic energy radiated by the field source, and the useless power loss. Loss of useless power includes resistive loss, mechanical friction loss, and dielectric loss. Resistive loss includes motor copper loss, controller and power converter loss, etc. Mechanical friction loss includes

Table 1: Parameter table of permanent magnet and exciting coil.

Model name	Permanent magnet	Exciting coil
Material	N52	Copper ($d = 2$ mm)
Circular section	3×10^{-3} m^2	3×10^{-3} m^2
Height	0.03 m	0.03 m
Shape	Cylinder	Cylinder

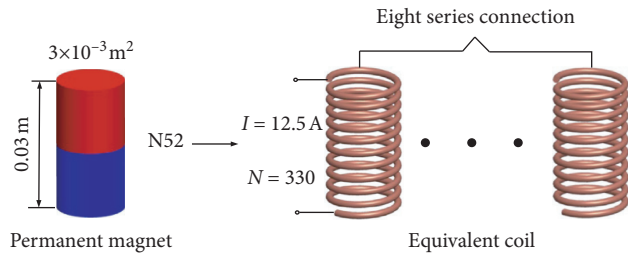

Figure 1: Model diagram of permanent magnet and the exciting coil.

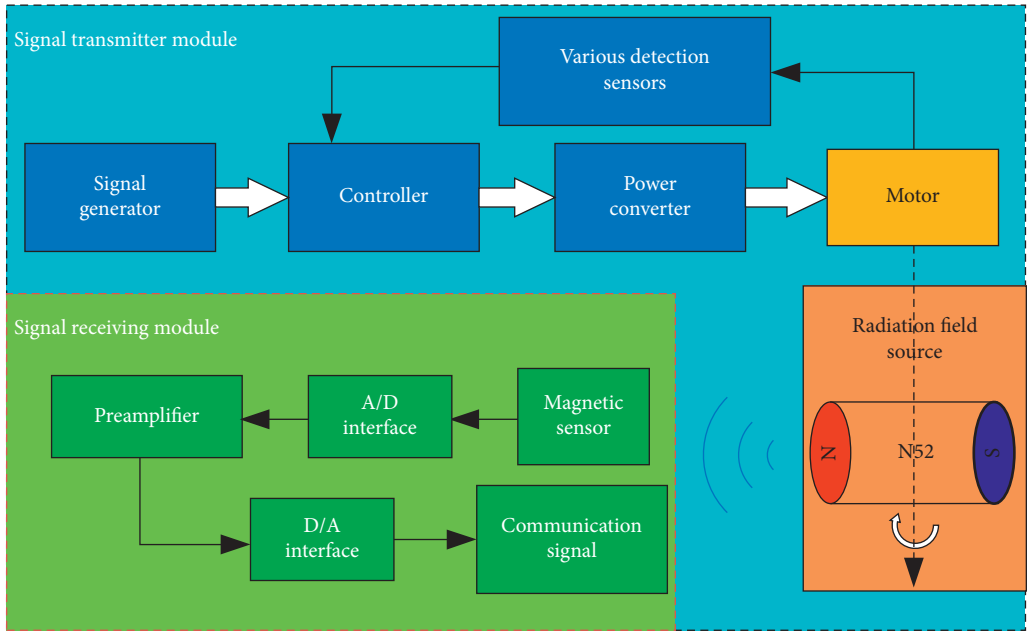

Figure 2: Schematic diagram of the mechanical antenna structure.

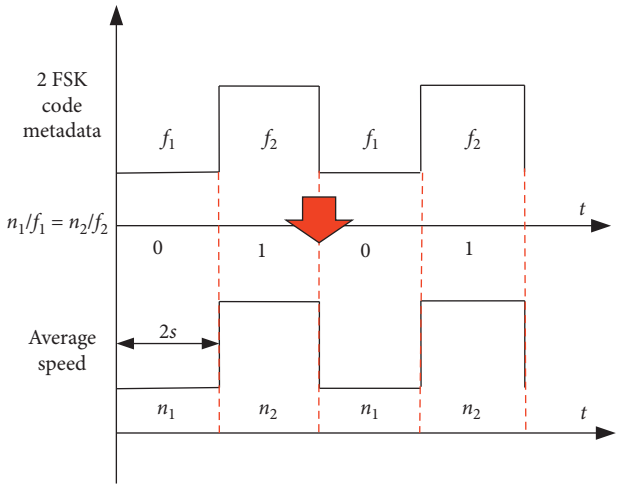

Figure 3: Schematic diagram of speed control signal generation for 2FSK.

overcoming friction caused by bearings, wind resistance, etc. Dielectric loss includes two parts, namely: (1) eddy current and hysteresis loss of the motor core; (2) near-field energy storage where a rotating field source generates a time-varying magnetic field. Therefore, the mechanical power output by the permanent magnet synchronous motor can be expressed as

$$P_M = P_{\text{in}} - P_R - P_\Omega - P_{m_1} = P_{m_2} + P_{\text{rad}}, \tag{2}$$

where P_R is resistive loss; p_Ω is mechanical friction loss; P_{m_1} is eddy current and hysteresis loss of the motor core; P_{m_2} is the dielectric loss of the time-varying electromagnetic field generated by the rotation of the field source; and P_{rad} is the radiated power.

According to the above energy conversion relationship, the radiation efficiency of the mechanical antenna can be defined as

$$\eta = \frac{P_{\text{rad}}}{P_{\text{in}}} = \frac{P_{\text{rad}}}{P_{m_2} + P_{\text{rad}} + P_R + P_\Omega + P_{m_1}}. \tag{3}$$

3. Research on Magnetic Field Distribution Characteristics and Magnetic Reception Technology

At present, magnetic reception technology is basically used for super-low-frequency electromagnetic communication. The development of a prototype mechanical antenna to meet the communication needs is the key to this study. In this study, the radiation intensity of rotating permanent magnets and the reception performance of magnetic sensors directly affect the communication distance. Therefore, it is crucial to study the time-varying magnetic field characteristics radiated by rotating permanent magnets as well as the magnetic sensor sensitivity. A theoretical reference is provided for the development of a high-performance mechanical antenna communication model.

3.1. Magnetic Field Distribution and Attenuation Characteristics of Rotating Permanent Magnets

3.1.1. Physical Model of Rotating Permanent Magnet. The physical model of the rotating permanent magnet is shown in Figure 4, assuming that the dimensions of the permanent magnet are l, w, and h. In an infinite uniform medium, the permanent magnet takes the geometric center as the origin and moves at a constant rotation around the z-axis with

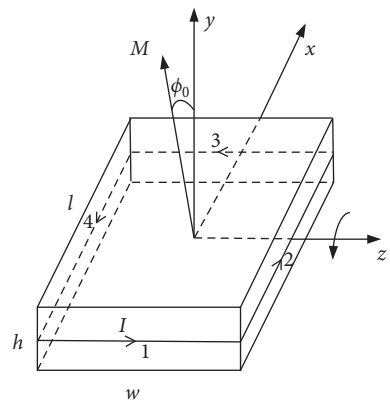

Figure 4: Diagram of rotating permanent magnet.

angular velocity ω. The angle between the direction of magnetization and the y-axis where the rotation begins is ϕ_0.

According to the ampere current model, the uniformly magnetized permanent magnet is equivalent to the ampere current on its surface. The direction of the current is shown in the direction of the arrow in Figure 4, and the equivalent surface current density is given:

$$\boldsymbol{\alpha} = \mathbf{M} \times \mathbf{n}, \tag{4}$$

where $\mathbf{M}$ is the equivalent surface current density constant and $\mathbf{n}$ is the unit vector of the magnetization direction of the permanent magnet itself.

In Figure 4, the surface currents are distributed on rectangular polar surfaces parallel to the direction of magnetization (the four faces labeled 1, 2, 3, and 4 in Figure 4), and there are no surface currents on the other faces.

3.1.2. Magnetic Field Distribution and Attenuation Characteristics. The equivalent current of a rotating permanent magnet is distributed only at its surface, and the retarded potential $\mathbf{A}$ ($\mathbf{r}$, t) is as follows:

$$\mathbf{A}(\mathbf{r}, t) = \frac{\mu}{4\pi} \iiint_{\Omega(t)} \frac{\mathbf{J}(\mathbf{r}', t - (R/c))}{R} \mathrm{d}V, \tag{5}$$

where μ is the magnetic permeability of the transmission medium; R is the distance between field point $\mathbf{r}$ and source point $\mathbf{r}'$; c is the speed of light; $\Omega(t)$ is the integral domain (four sides of 1, 2, 3, and 4 marked in Figure 4); and $\mathbf{J}$ ($\mathbf{r}'$, $t - R/c$) is the surface current density of source point $\mathbf{r}'$ at time $t' = t - R/c$.

For the permanent magnets shown in Figure 4, the retarded potential $\mathbf{A}$ ($\mathbf{r}$, t) can be deduced as follows:

$$\mathbf{A}(\mathbf{r}, t) = B_0 V e^{-j\phi_0} \frac{e^{j(kr - \omega t)}}{4\pi r^3} [-z(x + jy) + (x + jy)z(1 - jkr)], \tag{6}$$

where $B_0 = \mu M$ and V are the remanence and volume of the permanent magnet, respectively; $k = \omega/c$ is wave number.

Based on the retarded potential $\mathbf{A}$ ($\mathbf{r}$, t) and the ampere current model, the equations of magnetic induction intensity $\mathbf{B}$ ($\mathbf{r}$, t) and the electric field $\mathbf{E}$ ($\mathbf{r}$, t) of rotating permanent magnet at $\mathbf{r}$ are obtained:

$$\mathbf{B}(\mathbf{r}, t) = \nabla \times \mathbf{A}(\mathbf{r}, t) = \frac{B_0 V e^{j(kr - \omega t)}}{4\pi r^3} \left\{ -\mathbf{r}(2j + kr)\sin\theta + \boldsymbol{\theta}\left(j + 2kr - jk^2r^2\right)\cos\theta + \boldsymbol{\varphi}\left[-1 + \left(2jkr + k^2r^2\right)\cos^2\theta\right] \right\} e^{j(\phi - \phi_0)}, \tag{7}$$

$$\mathbf{E}(\mathbf{r}, t) = \frac{j}{\omega\varepsilon\mu} \nabla \times \mathbf{B}(\mathbf{r}, t) = j \frac{\eta M V e^{j(kr - \omega t)}}{4\pi r^3} \left\{ \mathbf{r} \frac{3}{2}(2 - jkr)\sin 2\theta + \boldsymbol{\theta}\left(-2 + 2jkr + k^2r^2\right)\cos^2\theta + \boldsymbol{\varphi}\left[-2j - \left(2kr - jk^2r^2\right)\cos\theta\right] \right\} e^{j(\phi - \phi_0)}, \tag{8}$$

where θ is the polar pole angle, which is the angle between the connecting direction of the test point and the origin and the positive direction of the z-axis; ϕ is the azimuthal angle, which is the angle between the connection direction of the test point and the origin and the positive x-axis direction; $\eta = \sqrt{\mu/\varepsilon}$ is the wave impedance of the transmission medium, where ε is the dielectric constant of the medium.

In the near field, $kr \longrightarrow 0$. From equations (7) and (8), the magnetic and electric field strengths in the near-field region can be expressed as follows:

$$\mathbf{B}_{\text{near}} = \frac{B_0 V e^{-j\omega t}}{4\pi r^3}\left\{-\mathbf{r}2j\sin\theta + \boldsymbol{\theta} j\cos\theta - \boldsymbol{\varphi}\cos^2\theta\right\}e^{j(\phi-\phi_0)}, \tag{9}$$

$$\mathbf{E}_{\text{near}} = j\frac{\eta M V e^{-j\omega t}}{4\pi r^3}\left\{\mathbf{r}3\sin 2\theta - \boldsymbol{\theta}2\cos^2\theta - \boldsymbol{\varphi}2j\cos\theta\right\}e^{j(\phi-\phi_0)}. \tag{10}$$

In the near field, the magnetic field strength $\mathbf{B}_{\text{near}}$ produced by the rotating permanent magnet has three components simultaneously $\mathbf{r}$, θ, and φ. The magnitude of the magnetic field strength is proportional to the remanence of the permanent magnet and decays in the third power of the communication distance r. The phase difference between the magnetic field intensity and the electric field intensity is $\pi/2$ in the near region, so the near-area field is a quasi-static field.

In the far field, $kr \gg 1$. From equations (7) and (8), the magnetic sand electric field strengths in the far-field region can be expressed as follows:

$$\mathbf{B}_{\text{far}} = \frac{B_0 V e^{j(kr-\omega t)}}{4\pi r}\left\{-\boldsymbol{\theta} jk^2\cos\theta - \boldsymbol{\varphi}\cos^2\theta\right\}e^{j(\phi-\phi_0)},$$

$$\mathbf{E}_{\text{far}} = j\frac{\eta M V e^{j(kr-\omega t)}}{4\pi r}\left\{-\boldsymbol{\theta} jk^2\cos^2\theta - \boldsymbol{\varphi}k^2\cos\theta]\right\}e^{j(\phi-\phi_0)}. \tag{11}$$

In the far field, the magnetic field strength $\mathbf{B}_{\text{far}}$ produced by the rotating permanent magnet has two components simultaneously θ and φ. In the far-field region, both the magnetic and electric field strength amplitudes decay with $1/r$ and are in phase. Thus, the far field is a spherical wave, with energy radiating out completely.

For a lossless medium, the radiation energy flow $\mathbf{S}$ of a rotating permanent magnet can be expressed as follows:

$$\mathbf{S} = \frac{1}{\mu}\left(\mathbf{E}_{\text{far}} \times \mathbf{B}_{\text{far}}\right) = -\frac{\eta B_0^2 V^2 e^{2j(kr-\omega t)}}{64\pi^2\mu r^2} jk^2\sin^2(2\theta))e^{2j(\phi-\phi_0)}. \tag{12}$$

In terms of the relationship between radiated power and energy flow density, the radiated power of a rotating permanent magnet can be expressed as follows:

$$\mathbf{P}_{\text{nrad}} = \int \mathbf{S}\mathrm{d}s = \oint |\mathbf{S}| r^2\sin\theta\mathrm{d}\theta\mathrm{d}\phi = \frac{\eta B_0^2 V^2}{32\pi^2\mu_0 r^4}, \tag{13}$$

$$\mathbf{P}_{\text{frad}} = \int \mathbf{S}\mathrm{d}s = \oint |\mathbf{S}| r^2\sin\theta\mathrm{d}\theta\mathrm{d}\phi = \frac{7\eta B_0^2 V^2}{480\pi^2\mu}. \tag{14}$$

From equation (13), the radiated power of the time-varying magnetic field generated by a rotating permanent magnet in the near field is proportional to the square of the residual magnetism and volume of the permanent magnet, and inversely proportional to the quartic of the communication distance. From equation (14), the radiated power of the time-varying magnetic field generated by the rotating permanent magnet in the far field is proportional to the square of the residual magnetism of the permanent magnet and the volume of the permanent magnet and is independent of the communication distance.

3.2. Sensitivity Study of Magnetic Sensor. From equation (9), a permanent magnet of material NdFeB, grade N52, remanence of 1.38 T, and size $\phi 100 \times 200$ mm produces a time-varying magnetic field strength of 125 fT at 1 km by rotational motion. Therefore, the resolution of the magnetic sensor in the mechanical antenna communication receiving unit needs to be 125 fT/$\sqrt{\text{Hz}}$ and the detectable magnetic field range needs to be less than 125 fT.

3.2.1. Magnetic Sensor Model. Today, the detectable range and resolution of standard magnetic sensors are shown in Table 2. From Table 2, it can be seen that the optimal magnetic sensors for the super-low-frequency time-varying magnetic field measurements are superconducting quantum interferometers and coils. Because of its simple structure, convenient construction, and stable performance, the coil has low requirements for SLF communication environment. It is convenient to build antenna communication structure. Therefore, in this study, the coil is selected as the SLF mechanical antenna signal receiving module.

According to the law of electromagnetic induction, the coil will generate an induced electric potential of the same frequency in the time-varying magnetic field of the transmitting antenna. The coil acts as a magnetic sensor, and its most sensitive direction is the normal direction. Therefore, the mechanical antenna communication system uses a three-axis orthogonal square coil for signal reception. The time-varying magnetic field in any direction in space is determined by detecting the time-varying magnetic field in the X, Y, and Z directions with a three-axis orthogonal coil.

3.2.2. Normalized Sensitivity Model of Magnetic Sensor Sensitivity. The super-low-frequency mechanical antenna adopts a three-axis orthogonal square coil magnetic signal receiving technology. The ability to develop a coil that meets the communication requirements is the key to this research. In a time-varying magnetic field, the induced voltage of the coil represents the average value of the detection signal, and the thermal noise voltage represents the minimum value of the detection signal. Therefore, in this study, the coil sensitivity was characterized by the equivalent ratio of antenna thermal noise voltage and time-varying magnetic field-induced voltage. The sensitivity normalization model is developed to provide the theoretical basis for the design of high-performance magnetic sensor coils.

(1) Time-Varying Magnetic Field-Induced Voltage. According to the principle of equivalent distribution of the electrical characteristic parameters of the coil, the equivalent resonance circuit model of the air-core coil is shown in Figure 5. In the figure, U is the output-induced voltage of the coil; R is the equivalent resistance of the coil, that is, the resistance of

Table 2: Detection range and resolution of typical magnetic sensor.

Magnetic sensor	Detectable filed range	Resolution
SQUID	100 fT~100 mT	~50 fT/Hz
Search coil	>50 fT	<100 fT/Hz
Flux-gate	1 nT~1 mT	~100 fT/Hz
Optical pump	500 fT~1 mT	~1 pT/Hz
GMR	>1 nT	~100 pT/Hz
Hall-effect	1 mT~50 T	~10 nT/Hz

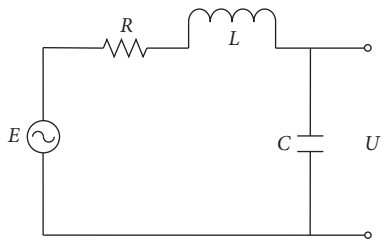

Figure 5: Air-core coil equivalent circuit diagram.

the wires that constitute the coil; L is the equivalent inductance of the induction coil, which represents the inherent characteristics of the coil itself and has nothing to do with the current; C is the equivalent capacitance of the coil, mainly the capacitance existing between the turns of the coil.

The time-varying magnetic field generated by a rotating permanent magnet is a sinusoidal signal whose output-induced voltage can be expressed as follows:

$$U = NA\omega B\cos(\omega t) = 2\pi f NAB\cos(\theta), \tag{15}$$

where N is the number of turns of the coil; A is the area of the single-turn coil; ω is the rotation angular velocity of the permanent magnet; f is the operating frequency of the rotating permanent magnet; θ is the angle between the incident direction of the time-varying magnetic field and the axis of the coil. When the coil axis is horizontal, θ only indicates the position of the receiver coil, and its value is 0°. Therefore, the cos (θ) in the formula (15) can be ignored.

It can be seen from equation (15) that the number of coil turns N, the coil area A, and the working frequency f are all proportional to the induction electromotive force of the coil.

(2) Thermal Noise Voltage. In the SLF domain, the wavelength (10^3 km~10^4 km) of the electromagnetic wave is much larger than the width of the coil. Therefore, the winding capacitance and surface skin effect of the coil can be ignored. The magnetic induction coil is equivalent to an inductive device consisting of a resistor and an inductor. Its equivalent circuit is shown in Figure 6. It consists of equivalent resistance R and equivalent inductance L.

According to the definition of resistance, the coil resistance can be expressed as follows:

$$R = \frac{4\rho N c_1\sqrt{A}}{\pi d^2}, \tag{16}$$

where ρ is coil resistivity; d is the wire diameter; N is the number of turns of the coil; and A is the cross-sectional area of the coil.

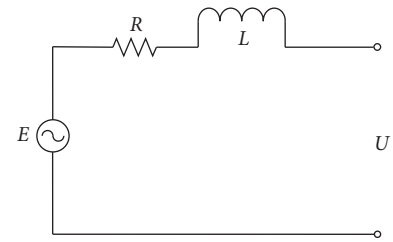

Figure 6: Equivalent circuit diagram of receiving coil.

According to Biot–Savart Law, the inductance L of coils of different shapes can be expressed as follows:

$$L = 2\times 10^{-7} N^2 c_1\sqrt{A}\left[\ln\frac{c_1\sqrt{A}}{\sqrt{N}\,d} - c_2\right], \tag{17}$$

where c_1 and c_2 are coil shape coefficients, and coil coefficients of different shapes are shown in Table 3.

In the super-low-frequency domain, the wavelength of electromagnetic waves (4000 km at 75 Hz) is much larger than the edge length of the coil, so the radiation resistance of the coil is negligible compared to the coil resistance. Therefore, the minimum value of the detection signal is limited by the thermal noise generated by the coil resistance R_a. The RMS (root mean square) thermal noise voltage V_{Nt} across the coil resistance R_a can be expressed as

$$U_{\mathrm{Nt}} = \sqrt{4KTR\Delta f}, \tag{18}$$

where K is Boltzmann constant, $K = 1.38\times 10^{-23}$ ws/K; T is the absolute temperature of the conductor (K); Δf is the noise bandwidth of the measurement system. The unit to the RMS thermal noise voltage is $V\cdot\sqrt{\mathrm{Hz}}$.

It can be seen from formula (18) that the main influencing factors of the coil thermal noise voltage are the coil resistance R and the noise bandwidth Δf.

(3) Sensitivity of Magnetic Induction Coil. The magnetic induction coil sensitivity S is defined as the field equivalent of the noise density, which is the equivalent ratio of the coil-induced electromotive force to the thermal noise voltage. In other words, the magnetic induction coil sensitivity is the magnetic field equivalent of the thermal noise in a 1 Hz bandwidth. Let the RMS thermal noise voltage of the 1 Hz bandwidth be equal to the output voltage to obtain the magnetic field intensity of the magnetic induction coil measurement signal. Therefore, the sensitivity of a magnetic induction coil can be expressed as

$$S = \frac{\sqrt{4KTR}}{2\pi f NA}. \tag{19}$$

It can be seen from equation (19) that the sensitivity of the receiving antenna increases with increasing frequency. However, frequency is an external factor that affects the sensitivity of the receiving antenna. In mechanical antenna communication, the presence of bandwidth can change the sensitivity of the same structural coil. In order to study the factors influencing the variation of coil sensitivity in the

Table 3: Coil shape coefficients of different shapes.

Shape of coil	c_1	c_2
Square	4.000	1.217
Equilateral triangle	4.559	1.561
Right isosceles triangle	4.828	1.696

same structure during communication, the coil sensitivity calculations were normalized with a normalization factor of $1/f$. Therefore, the normalized formula for coil sensitivity can be organized into equation (20), which has units of $T/\sqrt{\text{Hz}}$:

$$\widehat{S} = \frac{\sqrt{4KTR}}{2\pi NA}. \tag{20}$$

From equations (16) and (20), the relationship between the geometric parameters and sensitivity of the magnetic induction coil can be expressed as follows:

$$\widehat{S} = \frac{\sqrt{4KT\rho c_1}}{\pi^{3/2} d\sqrt{N} A^{3/4}}. \tag{21}$$

From equation (21), the factors that affect the sensitivity of the magnetic induction coil are the parameters of the coil itself. There is a correlation between coil sensitivity $\widehat{S}$ and its turns N, cross-sectional area A, and wire diameter d. Therefore, the coil sensitivity can be improved by increasing the number of turns, the cross-sectional area, and the wire diameter within the allowable coil size. Therefore, the design accuracy of the geometric parameters of the magnetic induction coil is directly related to the accuracy of the sensitivity of the coil model.

4. Simulation Analysis of Radiation Field Attenuation Characteristics

Super-low-frequency mechanical antennas are long-distance communication devices whose communication media are mainly air, soil, and seawater. In order to better study its propagation characteristics, this paper uses the simulation software Ansoft to simulate the attenuation characteristics of the radiation field in different media. The simulation model is shown in Figure 7. The parameters related to the transmission medium and the permanent magnet in the simulation model are shown in Table 4.

The simulation results are processed to obtain the radiation intensity at the corresponding detection points in different propagation media. The simulation results are processed to derive the distance-dependent curves of the magnetic induction intensity of rotating permanent magnets in the three propagating media, as shown in Figure 8. The propagation characteristic curve was fitted using Matlab for the transmission medium of air, and the results are shown in Figure 8.

It can be seen from Figure 8 that the radiation signal of the rotating permanent magnet has the least propagation loss in air, followed by soil, and the greatest propagation loss in seawater. In air and soil, the time-varying magnetic field generated by rotating permanent magnets had essentially the same trend. It is assumed that the minimum magnetic induction strength that can be detected by the receiving antenna is 1 nT. When the rotating permanent magnet operates at a frequency of 75 Hz, the maximum communication distance is 147.5 m in air, 145 m in soil, and 73 m in seawater. In fact, some SLF receivers can detect signals with a magnetic susceptibility of less than 1 nT. Therefore, the communication distance will be longer. From the fitted curve of the propagation medium being air, it is known that the magnetic susceptibility is inversely proportional to the cube of the propagation distance. It is proved that the mathematical model of the rotating permanent magnet is correct.

5. Principle Prototype Development and Experimental

Based on the mechanical antenna communication structure and magnetic induction coil, the principle prototype shown in Figure 9 was constructed. The principle prototype is composed of three main parts: the radiation unit, the propagation path, and the receiving unit. The mechanical antenna radiation unit transmits signals through a signal generator. The frequency converter receives signals from the signal generator to control the motor speed. The motor drives a permanent magnet that generates a time-varying magnetic field, which radiates electromagnetic waves. Electromagnetic waves propagate in the air or on the ground and are received by magnetic sensors. The mechanical antenna receiving unit receives the signal via a three-axis orthogonal coil. The coil receives the signal and transmits it to an oscilloscope, which converts the analog signal into a digital signal. Then, the digital signal is sent to the upper computer, and the upper computer performs Fourier transform on the signal to obtain the transmission signal information of the radiation unit, thereby completing the communication.

Based on the mechanical antenna communication principle prototype, experiments are conducted on the rotating permanent magnet radiation power, coil sensitivity, and 2FSK communication. A three-axis orthogonal square coil with an impedance of 1 Ω-1 mH is developed as the mechanical antenna receiving unit. The driving motor speed is 0~15,000 r/min, corresponding to the emitted electromagnetic wave is 0~250 Hz and continuously adjustable.

5.1. Radiation Power Influence Experiment. According to the communication principle model diagram of the mechanical antenna shown in Figure 9 and radiation power model (13), the super-low-frequency mechanical antenna experimental platform shown in Figure 10 is built to study the influence of the permanent magnet volume on the radiation power. The

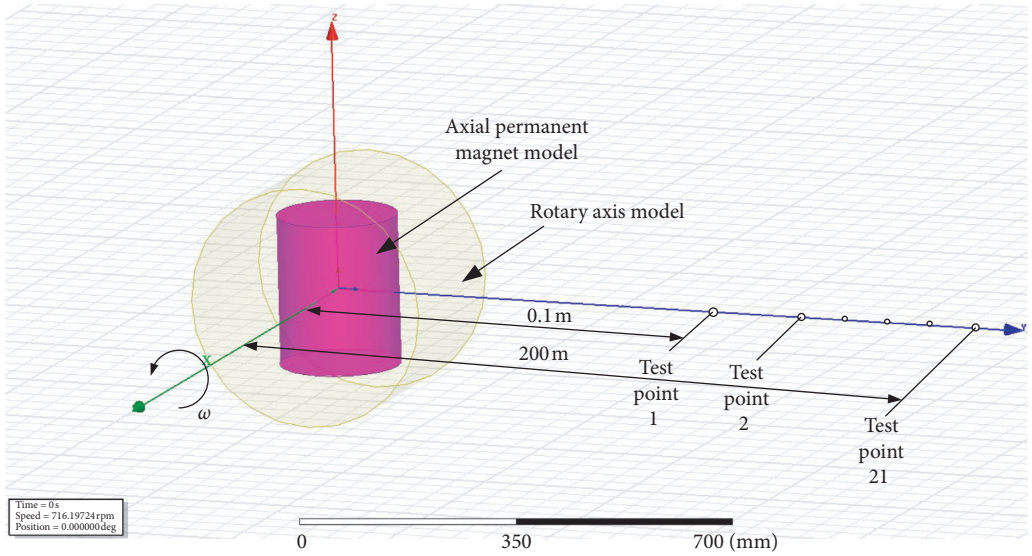

Figure 7: Simulation model of radiation field propagation characteristics of rotating permanent magnets.

Table 4: Simulation condition parameters.

Name of simulation parameters			Parameter values
Boundary environment	Air	Relative dielectric constant	1
		Conductivity (S/m)	0.0018
	Soil	Relative dielectric constant	13
		Conductivity (S/m)	0.001
	Sea water	Relative dielectric constant	81
		Conductivity (S/m)	4
Permanent magnet parameter		Relative permeability	1.05
		Mass density (kg/m^3)	7500
		Magnitude (kJ/m)	1.1×10^6
		Size	$\phi 200 \times 250$ mm

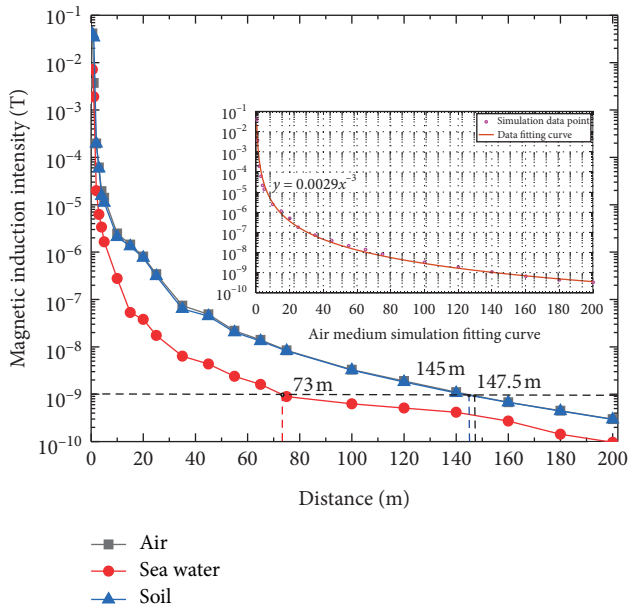

Figure 8: The change law of magnetic induction intensity of rotating permanent magnet.

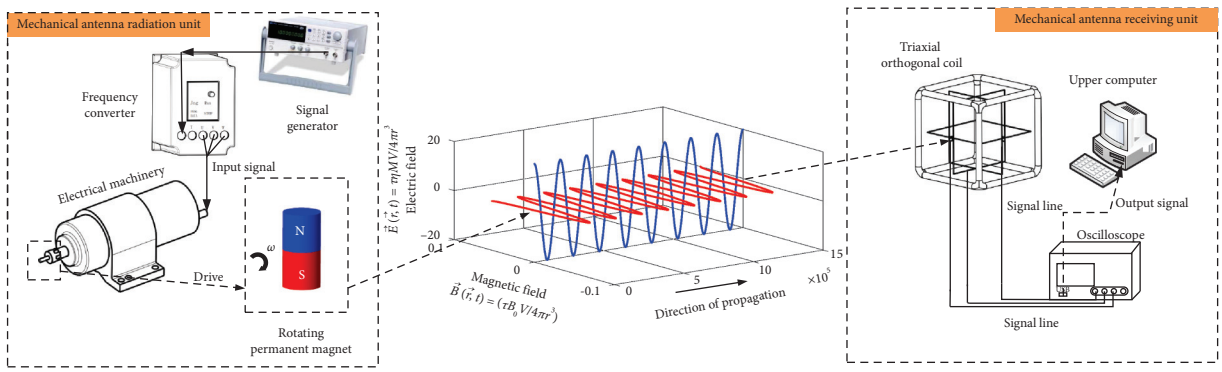

Figure 9: Mechanical antenna communication principle prototype.

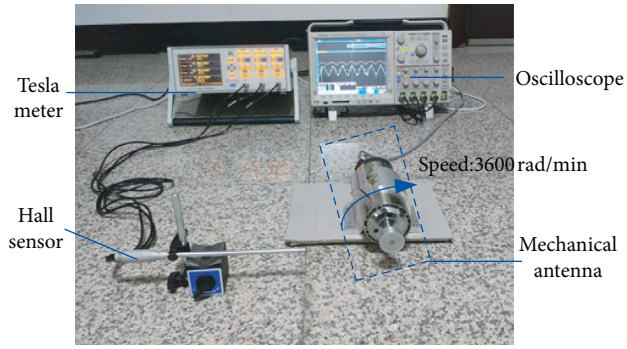

Figure 10: Principle prototype of super-low-frequency mechanical antenna.

driving motor speed is 3600 rad/min, and the corresponding electromagnetic wave radiation frequency is 60 Hz. The permanent magnet adopts 4 types of radially magnetized permanent magnets as shown in Table 5, and their time-varying magnetic field signals are measured, respectively. In this work, the time-varying magnetic field signals of 4 kinds of permanent magnets were analyzed to calculate their time-varying magnetic field magnetic induction intensity values, and their radiant power was calculated by combining equations (7) and (13). The permanent magnet model, time-varying magnetic field magnetic induction intensity, and radiation power are shown in Table 5. The radiant power generated by the rotating permanent magnet is fitted to the data with equation (13) using MATLAB to obtain the experimental fitting curve and experimental points as shown in Figure 11.

In this experiment, the four permanent magnets have the same material and magnetization capacity. In Figure 11, the experimental fitting curve is obtained by fitting the experimental points. The fitting curve equation is a unary quadratic function whose intercept is not zero. The relative error between the equation coefficient of the fitted curve and the theoretical value is 16.4%. The reason for the nonzero intercept of the equation is the error between the actual volume of the permanent magnet and the experimentally measured volume. The equation of the fitted curve is approximately the same as the radiated power resolution model, which shows that the radiated power of a rotating permanent magnet is proportional to the square of its volume. Therefore, its theoretical analytical model is reliable. Some factors that affect the communication distance of the mechanical antenna are as follows: the volume of the permanent magnet and the remanence of the permanent magnet.

5.2. Coil Sensitivity Influence Experiment. As shown in Figure 12, this paper builds a prototype coil sensitivity experiment based on a prototype mechanical antenna model. In Figure 12, *a* is the signal generator and frequency converter, and *b* is the motor and permanent magnet, which constitute the radiation unit; *c* is a three-axis orthogonal coil, and *d* is an oscilloscope, which constitute a receiving unit. In the radiation unit, a time-varying magnetic field is generated by a motor-driven permanent magnet, which forms electromagnetic waves. The frequency of electromagnetic waves is 75 Hz. The communication distance is set as 6 m. Radiation unit selected axially magnetized permanent magnet, which the material is N48, the remanence is 1.1 T, and the size is $90 \times \phi 8$ mm. According to equation (6), the theoretical value of time-varying magnetic field strength generated at 6 m on the rotating permanent magnet is $1.03\mu T$. The receiving unit adopts copper wire with diameter of 1 mm.

In this paper, the effects of coil turns and cross-sectional area on sensitivity are analyzed by the single-factor method. Make the coil impedance 1Ω mH and design coils 1, 2, and 3 according to equations (16) and (17). To study the effect of coil cross-sectional area on coil sensitivity, design coils 1 and 3, and change only the coil cross-sectional area *A*, while keeping other parameters unchanged. To study the effect of coil turns on coil sensitivity, design coils 2 and 3, and change only the coil turns *N*, while keeping other parameters unchanged. The detailed geometry of the coil is shown in Table 6.

The time-varying magnetic field is measured using coil 1, coil 2, and coil 3, respectively, and the induced voltage at 6 m is obtained in the time domain, and the frequency domain is obtained by FFT transformation of the time domain as shown in Figure 13. The RMS value of the induced voltage is shown in Table 7 in the time domain diagram, and the frequency domain diagram shows that the operating frequency of the time-varying magnetic field is 75 Hz, which is

Table 5: Radiation intensity and power of rotating permanent magnets.

Size (mm)	Volume (mm^3)	Magnetization direction	Magnetic field strength (T)	Experimental radiation power (W)
$5 \times 5 \times 20$	500	Radial	4.173×10^{-5}	1.304×10^{-9}
$20 \times \phi 6$	565		8.5×10^{-5}	6.107×10^{-9}
$30 \times \phi 5$	589		9.25×10^{-5}	7.578×10^{-9}
$30 \times \phi$	648		1.14×10^{-4}	1.263×10^{-8}

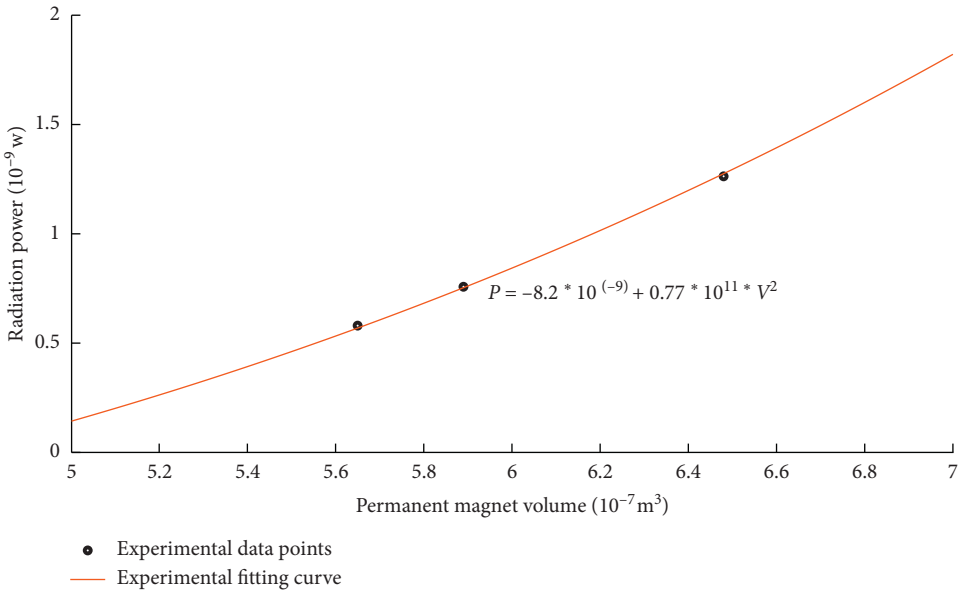

Figure 11: Curve diagram of the relationship between the volume and radiation power of rotating permanent magnet.

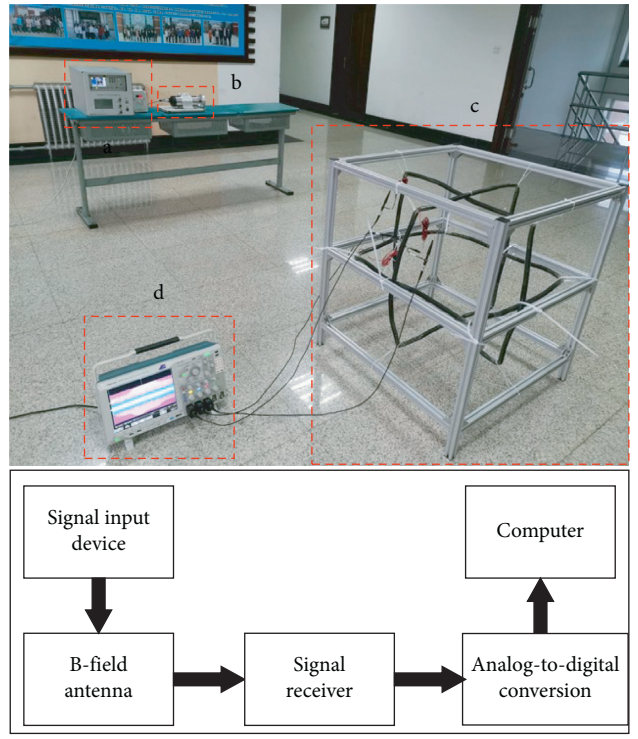

Figure 12: Photographs and block diagram of the mechanical antenna. (a) Signal input device, including signal generator and frequency converter; (b) B-field device, including motor, fixture, and permanent magnet; (c) signal receiver, consisting of three quadrate coils; (d) analog-to-digital conversion device: oscilloscope.

Table 6: Experimental coil parameters.

Parameters	Coil turns N	Coil length (m)	Coil diameter (mm)	Coil shape	Coil Impedance (Ω mH)
Coil 1	21	0.6	1	Square	1.03
Coil 2	11	1.68	1	Square	1.16
Coil 3	21	1.68	1	Square	0.86

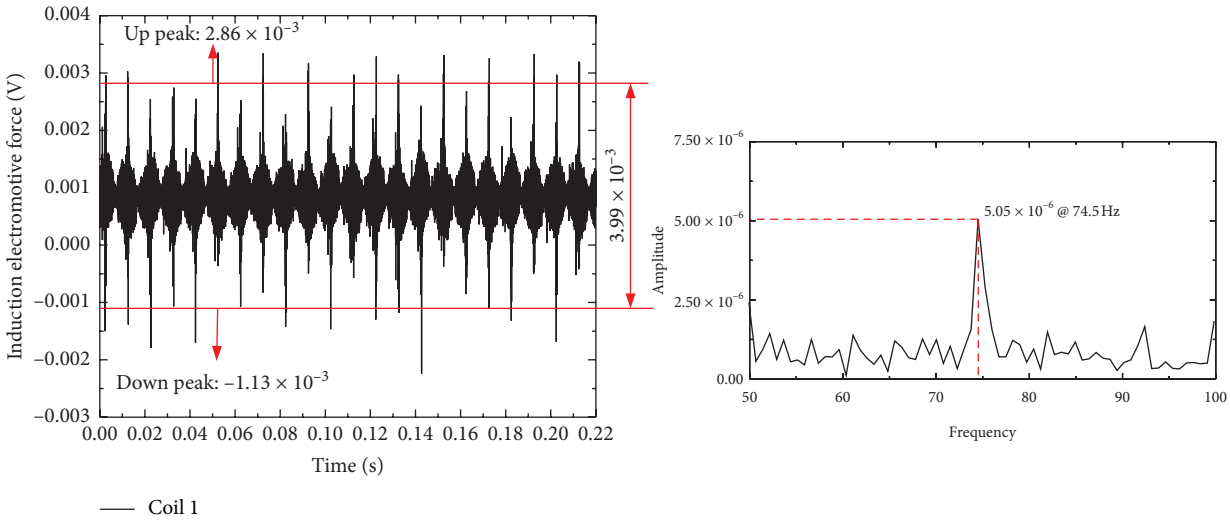

(a)

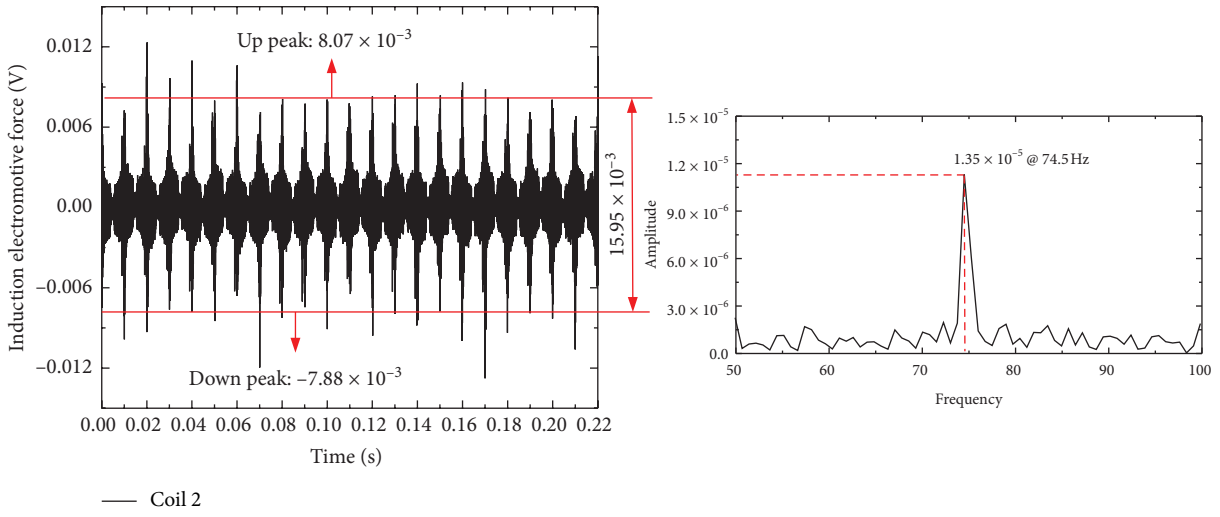

(b)

Figure 13: Continued.

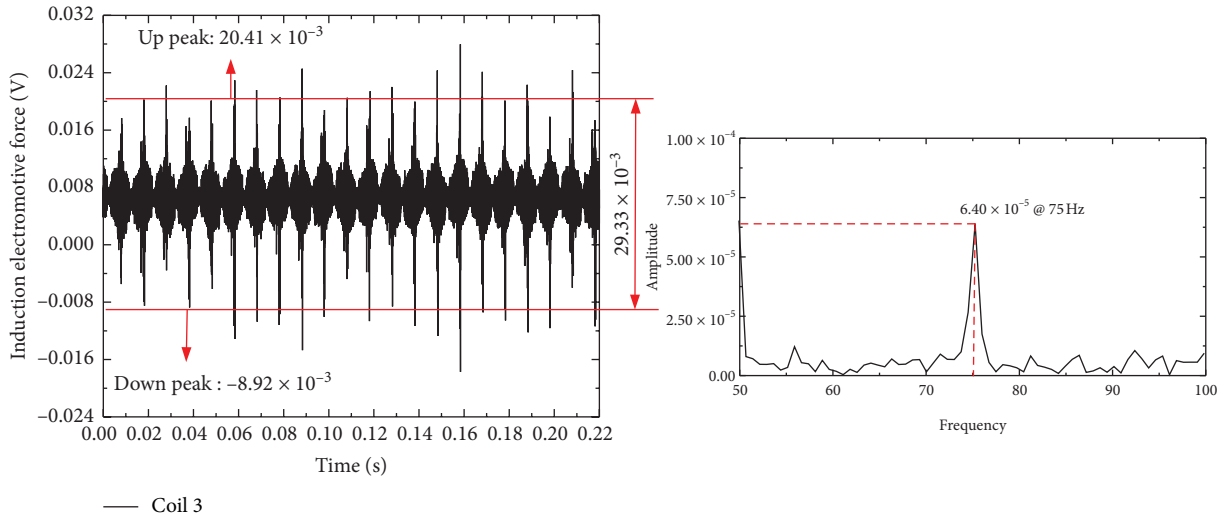

(c)

Figure 13: FFT diagram of the signal the coil at 6 m communication experiment.

Table 7: RMS of coil-induced voltage and time-varying magnetic field strength.

Coils	Effective value of induced voltage (mV)	Effective value of time-varying magnetic field strength (μT)	Theoretical value of time-varying magnetic field strength (μT)	Magnetic field strength error (%)
Coil 1	3.99	1.12	1.03	8.74
Coil 2	15.95	1.09	1.03	5.83
Coil 3	29.33	1.05	1.03	1.94

the same as the rotation frequency of the motor. From equation (15), the RMS value of the induced voltage of each coil was transformed into the RMS value of the time-varying magnetic field strength and compared with the theoretical value, and the results are shown in Table 7.

From the comparison between the experimental and theoretical values of coil 1 and coil 3 in Table 7, it can be seen that when the cross-sectional area of the coil increases from 0.36 m^2 to 2.82 m^2, the measurement error of the same time-varying magnetic field decreases by 6.8%. By comparing the experimental and theoretical values of coils 2 and 3, the number of coil turns increased from 11 to 21, and the time-varying magnetic field measurement error of the same target environment was reduced by 3.89%. Therefore, the coil sensitivity can be improved by increasing the coil cross-sectional area and turns. The measurement error of all three coils is less than 10%, which proves that the normalized analytical model of coil sensitivity is correct and can be used for the design of different models of magnetic induction coils for super-low-frequency mechanical antennas.

5.3. Communication Experiment. Antenna communication is through the coupling between the transmitting antenna and receiving antenna to complete the exchange and transmission of information. The modulation of the transmission signal has good penetration and stability in air and various media, and the signal is not easily distorted. 2FSK modulation is a binary digital frequency modulation, and the modulation method is shown in Figure 3. This study builds an experimental platform as shown in Figure 12 to simulate the signal modulation of 2FSK for wireless communication experiments.

The transmission signal is selected as a square wave signal as shown in Figure 14(a). Rotation frequencies of 60 Hz and 200 Hz correspond to input voltages of 0.5 V and 1.6 V, respectively. When the motor receives the input square wave signal, it drives the permanent magnet to rotate to form a radiation field, and the waveform diagram is shown in Figure 14(b). From 0 to 2.00 s, the input voltage of the motor is 1.6 V, and the radiation field frequency of the permanent magnet is 200 Hz. From 2.00 to 4.00 s, the input voltage of the motor is 0.5 V, and the radiation field frequency of the permanent magnet is 60 Hz. Therefore, the modulation rate is 70 Hz/s. The two waveforms correspond to the symbols 1 and 0 of the modulated signal. The waveform is processed by the short-time Fourier transform to obtain the time-frequency domain as shown in Figure 14(c).

As shown in Figure 14, the input signal waveform of the mechanical antenna communication system is almost identical to the time-frequency domain of the output signal. It can be seen from Figure 14(c) that the graph of the short-

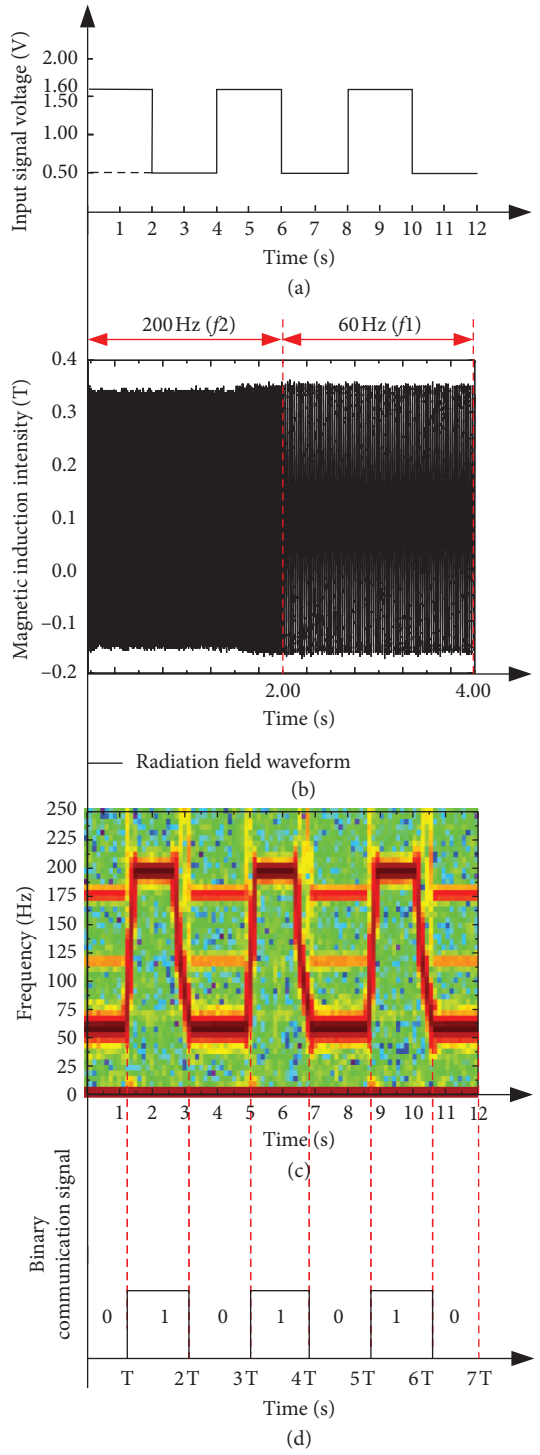

Figure 14: Waveform of the communication system: (a) input signal waveform; (b) waveform of received signal corresponding to frequency f_1 and f_2; (c) time domain diagram of received signal; (d) transmission signal waveform.

time Fourier transform has a certain slope when the frequency changes abruptly. Due to the transient nature of the speed of the drive motor, there is a process (Δt) of changing the frequency in the time-frequency domain diagram at the time of shear, making the frequency change at the slash. The frequency rise process time is 0.102 s, and the frequency fall process time is 0.205 s. The total change process is $\Delta t = 0.307$ s, so the bit-error rate of the source in the 2FSK communication system is 7.68%. The experimental results are the same with the preset condition trends and values, which verifies the effectiveness and feasibility of the rotating permanent magnet-based super-low-frequency mechanical antenna communication method described in this paper from the practical application level.

6. Conclusions

Traditional SLF antennas are bulky, power-consuming, and inefficient. This paper introduces a mechanical antenna with a rotating permanent magnet as a radiation element and a triaxial orthogonal coil as a receiving element. For radiation unit, a mathematical model based on rotating permanent magnet and radiation power is established. For the receiving unit, a mathematical model based on the dimension parameters and sensitivity of the square coil is established. According to the analysis of theory, simulation, and experimental results, some characteristics of the mechanical antenna communication mechanism are obtained as follows:

(1) For the radiating element of a mechanical antenna, the near-field radiated power is proportional to the square volume of the permanent magnet. Increasing the volume of the permanent magnet can increase the radiated power, thus increasing the communication distance.

(2) For mechanical antenna receiving unit, coil sensitivity is proportional to the number of turns and area of the coil. Increasing the coil area and turns can improve the receiving antenna sensitivity, so as to increase the communication distance.

(3) The communication experiments of the mechanical antenna show that the mechanical antenna can be used for wireless communication. In addition, the modulation of the 2FSK signal can be realized by real-time control of the motor speed. The modulation rate is 70 Hz/s, and the bit-error rate is 7.68% during communication.

From above, the mechanical antenna subverts the excitation of ultra-low-frequency electromagnetic waves. However, compared with the existing ESA technology, the mechanical antenna cannot significantly increase the effective radiated power under the same dipole moment condition. Now, mechanical antenna is difficult to replace the existing high-power transmitter. At present, the research on mechanical antenna at home and abroad mainly focuses on radiation excitation, realization mode, and experimental verification.

Data Availability

The data used to support the findings of this study are included within the article.

Conflicts of Interest

The authors declare that they have no conflicts of interest.

Acknowledgments

This work was supported by the National Natural Science Foundation of China (no. 51775078), Opening Fund of National Center for International Research on Structural Health Management of Critical Components (no. KFJJ20-02K), and National Natural Science Foundation of China (no. 51005029).

References

[1] C. Liu, L. G. Zheng, and Y. P. Li, "Study of ELF electromagnetic fields from a submerged horizontal electric dipole positioned in a sea of finite depth," in *Proceedings of the 2009 3rd IEEE International Symposium on Microwave, Antenna, Propagation and EMC Technologies for Wireless Communications*, pp. 152–157, Beijing, China, October 2009.

[2] R. Barr, W. Ireland, and M. J. Smith, "ELF, VLF and LF radiation from a very large loop antenna with a mountain core," *IEE Proceedings H Microwaves, Antennas and Propagation*, vol. 140, no. 2, pp. 129–134, 1993.

[3] M. Alibakhshikenari, B. S. Virdee, A. Ali et al., "Extended aperture miniature antenna based on CRLH metamaterials for wireless communication systems operating over UHF to C-band," *Radio Science*, vol. 53, no. 1-2, pp. 154–165, 2018.

[4] M. Alibakhshikenari, B. S. Virdee, L. Azpilicueta et al., "A comprehensive survey of "metamaterial transmission-line based antennas: design, challenges, and applications," *IEEE Access*, vol. 8, pp. 144778–144808, 2020.

[5] M. Alibakhshikenari, B. S. Virdee, and E. Limiti, "Compact single-layer traveling-wave antenna design using metamaterial transmission lines," *Radio Science*, vol. 52, no. 11-12, pp. 1510–1521, 2017.

[6] C. Simovski, A. Miroshnichenko, and P. Belov, "Comment on "electromagnetic radiation under explicit symmetry breaking"" *Physical Review Letters*, vol. 114, no. 14, Article ID 147701, 2015.

[7] T. Nan, H. Lin, and Y. Gao, "Acoustically actuated ultra-compact NEMS magnetoelectric antennas," *Nature Communications*, vol. 8, no. 1, p. 296, 2017.

[8] Z. Yao, Y. E. Wang, S. Keller, and G. P. Carman, "Bulk acoustic wave-mediated multiferroic antennas: architecture and performance bound," *IEEE Transactions on Antennas and Propagation*, vol. 63, no. 8, pp. 3335–3344, 2015.

[9] Y. Bin and H. Zhong-Qiang, "Recent progress of multiferroic magnetoelectric devices," *Acta Physica Sinica*, vol. 67, no. 15, Article ID 157507, 2018.

[10] M. A. Kemp, F. Matt, and A. Haase, "A high Q piezoelectric resonator as a portable VLF transmitter," *Nature Communication*, vol. 10, no. 1, p. 1715, 2019.

[11] J. A. Bickford, A. E. Duwel, M. S. Weinberg, R. S. McNabb, D. K. Freeman, and P. A. Ward, "Performance of electrically small conventional and mechanical antennas," *IEEE Transactions on Antennas and Propagation*, vol. 67, no. 4, pp. 2209–2223, 2019.

[12] S. Wei, Z. Qiang, and L. Bin, "Performance analysis of spinning magnet as mechanical antenna," *Acta Physica Sinica*, vol. 68, no. 18, Article ID 188401, 2019.

[13] A. Madanayake, S. Choi, and M. Tarek, "Energy-efficient ULF/VLF transmitters based on mechanically-rotating dipoles," in *Proceedings of the Moratuwa Engineering Research Conference (MERCon)*, pp. 230–235, Moratuwa, Sri Lanka, May 2017.

[14] M. N. Srinivas Prasad, Y. Huang, and Y. E. Wang, "Going beyond Chu Harrington limit: ULF radiation with a spinning magnet array," in *Proceedings of the IEEE International Symposium on Antennas and Propagation & USNC/URSI National Radio Science Meeting*, pp. 268–270, Montreal, QC, Canada, August 2017.

[15] S. Gong, Y. Liu, and Y. Liu, "A rotating-magnet based mechanical antenna (RMBMA) for ELF-ULF wireless

communication," *Progress in Electromagnetics Research M*, vol. 72, pp. 125–133, 2018.

[16] M. Chen, G. Han, and P. Guo, "A simple method for deriving electromagnetic radiation from uniform rotating electric dipole," *University Physics*, vol. 29, no. 11, pp. 23–25, 2010.

[17] A. E. Mahdi, L. Panina, and D. Mapps, "Some new horizons in magnetic sensing: high-Tc SQUIDs, GMR and GMI materials," *Sensors and Actuators A: Physical*, vol. 105, no. 3, pp. 271–285, 2003.

[18] Y. Shao and K. Song, "Study on inductance of wide-band inductive magnetic induction coil," *Journal of Electronic Measurement and Instrumentation*, vol. 28, no. 7, pp. 703–709, 2014.

[19] D. Wu, T. He, X. Wang, and Y. Huang, "A new analytical modeling method for impedance analysis of Arbitrary orthogonal polyline Coils using vertex configuration description," *Acta Electronic Sinica*, vol. 46, no. 9, pp. 2094–2101, 2016.

[20] P. Zhao, Y.-z. Jiang, S.-x. Zhang, and W.-w. Ying, "Design of the magnetic field sensing system for downlink signal reception and interference cancelling for through-the-earth communication," *Journal of Magnetics*, vol. 21, no. 3, pp. 330–339, 2016.

[21] X. Zhang, B. Wu, X. Liu et al., "Research on the electrical characteristics of electromagnetic induction coils," *Chinese Journal of Electrical Engineering*, vol. 39, no. 13, pp. 3963–3970, 2019.

[22] S. Tumanski, "Induction coil sensors—a review," *Measurement Science and Technology*, vol. 18, no. 3, pp. 31–46, 2007.

[23] H. C. Burch and A. Garraud, "Experimental generation of ELF radio signals using a rotating magnet," *IEEE Transactions on Antennas and Propagation*, vol. 1, no. 1, pp. 1–8, 2018.